# Fragmentation Dynamics of $CS_2$ Dications and Tricications Following S 2p Ionization

Felix Allum,[1,2,3] Chow-shing Lam,[4] Benjamin Erk,[1] Hubertus Bromberger,[1] Philip H. Bucksbaum,[3,5,6] Mathew Britton,[2,3] Michael Burt,[4,7] Nagitha Ekanayake,[1] Ian Gabalski,[3,5] Diksha Garg,[1] Eva Gougoula,[1] David Heathcote,[4] Andrew J. Howard,[3,5,8] Paul Hockett,[9] David M. P. Holland,[10] Sonu Kumar,[1,11] Jason W. L. Lee,[1] Joseph McManus,[4] Jochen Mikosch,[12] Dennis Milešević,[4] Russell S. Minns,[13] Christina C. Papadopoulou,[1] Christopher Passow,[1] Weronika O. Razmus,[13] Anja Röder,[14] Daniel Rolles,[15] Arnaud Rouzée,[14] Michael Schuurman,[9,16] Alcides Simao,[17] Albert Stolow,[9,16,18,19] Atia-Tul-Noor,[1] James Unwin,[4] Claire Vallance,[4] Tiffany Walmsley,[4] Mark Brouard,[4] and Ruaridh Forbes[2,8]

[1)]*Deutsches Elektronen-Synchrotron DESY, Notkestr. 85, 22607 Hamburg, Germany*

[2)]*Linac Coherent Light Source, SLAC National Accelerator Laboratory, Menlo Park, CA 94025, USA*

[3)]*Stanford PULSE Institute, SLAC National Accelerator Laboratory, Menlo Park, CA 94025, USA*

[4)]*Chemistry Research Laboratory, Department of Chemistry, University of Oxford, Oxford, OX1 3TA, UK*

[5)]*Department of Applied Physics, Stanford University, Stanford, CA 94305-4090, USA*

[6)]*Department of Physics, Stanford University, Stanford, CA 94305-4013, USA*

[7)]*Department of Chemistry, Trent University, 1600 West Bank Drive, Peterborough, K9L 0G2, ON, Canada*

[8)]*Department of Chemistry, University of California, Davis, CA 95616, USA*

[9)]*National Research Council Canada, 100 Sussex Drive, Ottawa, Ontario, K1A 0R6, Canada*

[10)]*Daresbury Laboratory, Daresbury, Warrington, Cheshire WA4 4AD, UK*

[11)]*Department of Physics, Universität Hamburg, Jungiusstraße 9, 20355 Hamburg, Germany*

[12)]*Institut für Physik, Universität Kassel, Heinrich-Plett-Straße 40, 34132 Kassel, Germany*

[13)]*School of Chemistry and Chemical Engineering, University of Southampton, Highfield, Southampton, SO17 1BJ, UK*

[14)]*Max-Born-Institute, Max-Born-Straße 2A, 12489 Berlin, Germany*

[15)]*J. R. Macdonald Laboratory, Department of Physics, Kansas State University, Manhattan, Kansas 66506, USA*

[16)]*Department of Chemistry and Biomolecular Sciences, University of Ottawa, 150 Louis Pasteur, Ottawa, Ontario, K1N 6N5, Canada*

[17)]*Ruhr-Universität Bochum, Fakultät für Chemie und Biochemie, Organische Chemie II, Universitätsstraße 150, 44801 Bochum, Germany*

[18)]*Department of Physics, University of Ottawa, 150 Louis Pasteur, Ottawa, Ontario, K1N 6N5, Canada*

[19)]*NRC-uOttawa Joint Centre for Extreme Photonics, Ottawa, ON K1A 0R6, Canada*

(*Electronic mail: ruforbes@ucdavis.edu)

(*Electronic mail: felix.allum@desy.de)

(Dated: 4 December 2025)

We present the results from a detailed study of the fragmentation dynamics of $CS_2^{2+}$ and $CS_2^{3+}$, formed in intense femtosecond soft X-ray pulses above the sulfur 2p edge, primarily through single core photoionization from the S 2p site, and subsequent Auger-Meitner decay(s). By combining three-dimensional velocity map imaging with covariance analysis, we determine the relative momenta of the ions produced in each two- and three-body fragmentation channel, at significantly higher ion count rates than conventional coincidence measurements. We shed new light on the wide range of fragmentation channels observed from the $CS_2$ dication and trication, including channels that involve ionization-induced bond formation and fragmentations producing undetected neutral cofragments. In the latter case, a 'native frames' approach is used to isolate contributions from concerted and sequential fragmentations and extract dynamical information about each step of a concerted fragmentation process. While dications often fragment sequentially, the trication is dominated by concerted fragmentation. The main trication fragmentation channel into $S^+ + C^+ + S^+$ can be well-approximated by classical Coulombic simulations of the ground-state geometry distribution, reflecting both the nature of the trication potential energy surface and the rapid multiple ionization prior to substantial structural dynamics. This study demonstrates ways in which fundamental insights into the fragmentation dynamics of polycations following X-ray ionization may be extracted, as will beneficial to future studies that employ time-resolved X-ray Coulomb explosion imaging to study ultrafast photochemistry.

## I. INTRODUCTION

The interaction between X-ray photons and molecules is of critical importance in a range of contexts, such as in understanding radiation damage in biological matter[1] or the evolution of chemical species in astrophysical environments[2]. X-ray interactions with matter are also extensively used as probes of molecular structure, for instance through spectroscopic[3] or diffractive imaging techniques[4]. Importantly, X-ray light interacts with core orbitals within molecules, enabling localized and site-selective spectroscopic probing[3]. The development of X-ray free-electron lasers (FELs) has enabled the extensions of such techniques to the ultrafast regime[5]. This has led to recent demonstrations of X-ray probing of ultrafast processes, such as photochemical reactions, in some cases yielding dynamical insights that could not be gleaned from traditional optical spectroscopies[6–8].

In many cases, the application of these emerging experimental techniques requires a detailed understanding of the dynamics initiated by X-ray photoabsorption. Of particular relevance to the current work is the technique of time-resolved X-ray induced Coulomb explosion imaging, in which a short X-ray pulse is used to produce and rapidly fragment a molecular polycation[9–11]. From the relative momentum distributions of the resultant fragment ions, structural information about photoexcited species can be determined. Typically, the analysis of such Coulomb explosion imaging experiments assumes a concerted fragmentation process, which is driven primarily by Coulombic forces[12]. Our understanding of when such approximations are valid, and how fragmentation occurs in polycations, is greatly informed by ion imaging studies in which the relative momenta of the different ions produced in a given fragmentation can be determined.

As a simple polyatomic molecule, the ionization and fragmentation dynamics of $CS_2$ have been studied extensively. In past work, multiple ionization has been induced in a range of regimes, such as: electron impact ionization[13]; heavy ion impact[14]; strong-field ionization[15–18] and single-photon inner-shell excitation from, or ionization of, core orbitals[19–23]. This work has explored vast regions of parameter space, spanning total charge states from +1 to +10, and consequently a large number of fragmentation channels. One key aspect of the dynamics explored in prior work is the coexistance of sequential and concerted fragmentation pathways, which has been interrogated in detail[16,23]. In the current work, we refer to two-step fragmentations via a long-lived intermediate (relative to its rotational timescale) as 'sequential', while fragmentations in which all bonds are broken simultaneously as 'concerted'. Fragmentations in between these two extremes are termed 'asynchronous'[24].

In general, while concerted fragmentations seem to dominate the dynamics of $CS_2^{n+}$ polycations, sequential fragmentation can be a significant pathway for low charge states (e.g. $n = 3$[16] or 4[23]). As $CS_2^{2+}$ dications are known to undergo three-body fragmentations[19,21,25], one might expect a similar competition between sequential and concerted breakup, but this has not yet been explored in detail.

In this work, multiple ionization and fragmentation of $CS_2$ is initiated by intense femtosecond soft X-ray pulses produced by the FLASH FEL[5], just above the S 2p ionization edge. Using three-dimensional velocity map imaging (VMI) and covariance analysis[26], we can isolate signals from individual fragmentation channels, with total charges ranging from +2 to +10. This approach enables us to determine the relative momenta of the ions produced in each fragmentation channel in the high-count-rate regime ($\sim$85 ions per shot). In the present work, we solely focus on the fragmentation dynamics of $CS_2^{2+}$ and $CS_2^{3+}$, which can be formed by a single S 2p photoionization. The fragmentation dynamics of higher total charge states, formed by multiple photoabsorption events within the pulse, will be explored in a separate publication[27]. We observe a range of two- and three-body fragmentation channels, including those which have been largely neglected in previous work. This includes a channel which involves rearrangement and bond formation within the dication to yield molecular $S_2^+$ and atomic $C^+$. For dications especially, the three-body fragmentation dynamics are shown to be rich and complex, and are characterized by the coexistence of sequential and concerted channels. Using recently developed native frames analysis techniques[26,28–30], we can interrogate these channels in great detail, clarifying aspects of their dynamics. Trications are found to undergo predominantly three-body fragmentation, primarily into $S^+ + C^+ + S^+$, although channels which yield asymmetric charge distributions are also observed. The momentum distribution arising from the $S^+ + C^+ + S^+$ channel agrees relatively well with classical Coulombic simulations of the ground-state geometry, indicating that core ionization and Auger-Meitner (AM) decays rapidly populate the unstable trication before substantial structural dynamics.

## II. METHODS

### A. Experimental Setup

Experiments were performed at the Free-electron LASer in Hamburg (FLASH), using the CAMP@FLASH instrument[31] at beamline BL1[5]. The CAMP@FLASH instrument, which comprises a dual-sided velocity map imaging spectrometer, was previously described in detail[31]. The experimental setup for the work described here is the same as our recent publications on time-resolved measurements of the dynamics of $CS_2$ induced by 200 nm photoexcitation[10,32]. In order to perform these pump-probe experiments using the FLASH1 optical laser, the FEL was operated in 'single bunch mode', corresponding to a repetition rate of 10 Hz.

Neat $CS_2$ was delivered as a continuous supersonic molecular beam into the center of the CAMP VMI spectrometer. The molecular beam was crossed by soft X-ray pulses produced by FLASH. The resultant cations and electrons were velocity-mapped to detectors at opposite ends of the spectrometer, each of which consists of two stacked micro-channel plates (MCPs) and a P47 phosphor screen. The electron imaging data are not

considered in this work. The flashes of light produced by ion impacts on the MCP/phosphor screen on the ion side of the spectrometer were recorded using a Timepix3 camera (Amsterdam Scientific Instruments)[33,34]. Importantly, the camera's 256 × 256-pixel sensor can also record the time of arrival and time over threshold of each event with a 1.56 ns and 25 ns resolution, respectively[33,35]. From these data, we can determine the corresponding time-of-flight (i.e. the timing of a detector event with respect to the FEL pulse). The temporal and spatial resolution of the Timepix data was improved via centroiding, as described previously by Bromberger *et al.*[34]. The $x$ and $y$ detector positions for each identified event, together with the time of flight, were used to determine the three-dimensional momentum of each detected ion. Contributions to these momenta arising from the initial velocity of the molecular beam were subtracted. Calibration to absolute momenta was performed using ion trajectory simulations in SIMION 8.1[36].

The intense soft X-ray pulses produced by FLASH had a central photon energy of approximately 180 eV, lying above the S 2p edge of $CS_2$[37] at around 170 eV. The average pulse energy measured by the FLASH Gas Monitor Detector (GMD)[38] for the data analyzed here was 54 μJ. Taking into account the estimated losses from transmission along the beamline, this corresponds to 23 μJ in the interaction region of the spectrometer. As detailed shortly, the shot-to-shot pulse energy measured by the GMD was included in the data analysis procedure. The duration of the intense soft X-ray pulses was estimated to be approximately 90 fs, based on the electron bunch charge, photon spectra, and transverse deflecting cavity ('LOLA') measurements[39]. The X-rays were focused into the interaction region using a pair of Kirkpatrick-Baez mirrors, achieving an estimated focal spot size of 10 μm[31]. Combining the estimated on-target pulse energy, duration, and spot size gives a peak intensity of $\sim 6\times10^{14}$ Wcm$^{-2}$, assuming a Gaussian spot.

The analyzed data were recorded during a UV (∼200 nm) – X-ray pump-probe experiment[10,32]. To obtain best statistics from the available dataset for analyzing the X-ray induced fragmentation, while avoiding including any UV pump – X-ray probe signal, the dataset used for the analysis herein was chosen to include both X-ray only data, and pump-probe data[10,32] for which the X-rays arrive 'early' (at least 100 fs prior to the UV). As shown in the Supplementary Material (SM Fig. S3), the weak (∼0.2 μJ) UV pulse alone produces predominantly bound $CS_2^+$ ions, with a small contribution of low kinetic energy $CS^+$ and $S^+$ ions from dissociative ionization. These low energy ions do not contribute to any covariance signals, as they originate from a monocation and so not from the correlated production of multiple fragment ions. To assess the possible role of any UV post-ionization of fragments produced by the X-ray ionization, we compare the momentum distributions and intensities of all fragment ions in X-ray only data and the X-ray early data with the UV pulse present (SM Figs. S3 and S4). The extreme similarity of data taken under these conditions suggests negligible contribution of UV post-ionization of fragments produced in the interaction with the X-ray pulse, and so the data analyzed reflects the outcome of the $CS_2$ sample interacting solely with the X-rays. ~~Given the low intensity of the UV pulse, we do not expect the UV pulse to induce any further ionization of charged fragments produced by the X-ray pulse. This is supported by comparing the momentum distributions and intensities of all fragment ions in X-ray only data and the X-ray early data with the UV pulse present (SM Figs. S3 and S4).~~ The total dataset analyzed comprises ∼320,000 shots and ∼27,000,000 ion events, corresponding to slightly over 8 hours of data acquisition at 10 Hz.

## B. Data Analysis and Simulations

### 1. *Covariance Calculations*

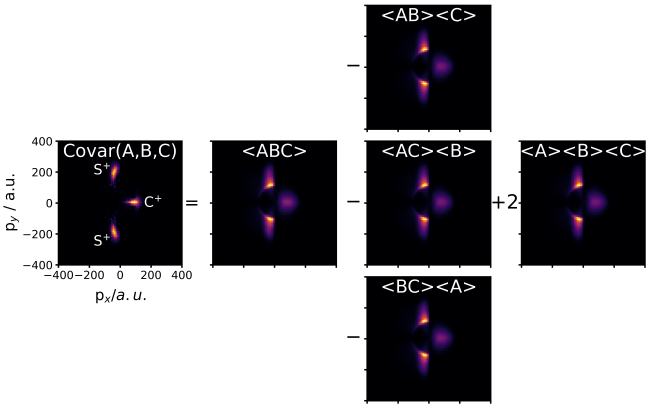


FIG. 1. Demonstration of the three-fold covariance imaging methodology. The left hand image shows the ($S^+$, $C^+$, $S^+$) covariance, plotted in the Newton frame described in the main text. The constituent terms used to calculate this three-fold covariance image are also each displayed.

The correlated momenta of the ions in a given dissociation are sensitive probes of the underlying fragmentation dynamics. Typically in ion imaging experiments, these physically meaningful correlations are extracted by performing experiments under 'coincidence conditions', where ions detected from the same laser shot can be assumed to come from the same molecule. In this regime, count rates are typically limited to the order of 0.1 to a few ions per shot. As count rates are raised, the relative contribution of 'false coincidences', i.e. uncorrelated signals arising from ionization of multiple parent molecules in a single laser shot, increases. This issue is particularly severe when detection efficiencies are limited, as is the case for ion detection with MCP detectors[40,41]. In the present work, we acquire data at far higher count rates (∼85 ions per shot) than those employed in coincidence experiments, and extract correlated information using covariance analysis. We have recently demonstrated and applied this methodology in several three-dimensional VMI experiments[10,29,42–44], and demonstrated the ability to extract high quality correlated ion momentum distributions with substantially reduced data acquisition times[26].

Covariance is a measure of the linear correlation between variables. Conceptually, covariance analysis, as applied in the current work, can be thought of as a procedure to subtract expected 'false coincidence' contributions from a given coincidence image. In the present work, two-[45,46] and three-fold[45,47] covariances between recorded ion momenta are calculated using the PyCorrCPI Python package[48], which takes advantage of recently suggested computational optimizations[49] and supports a flexible and customizable range of ways to represent the correlated momenta. The procedure of computing a three-fold covariance momentum map is illustrated in Fig. 1, as is the equation defining a three-fold covariance. In this example, the correlated momentum distribution between three ions ($S^+$, $C^+$, $S^+$) is represented as a Newton plot. Here, for each set of coincident ions, the $x$ axis is defined by the bisector of the two $S^+$ momenta, and the relative momenta of all ions are plotted in the $xy$ plane, such that each ion's $z$ momentum is zero.

For a complete dissociation channel, such as breakup into $S^+ + C^+ + S^+$, in which the momenta of all product species are recorded and correlated, the signal-to-noise of the covariance map can be improved by using momentum conservation[42,44]. Here, we filter on coincident ions whose summed momenta is almost equal to that of the neutral molecule prior to laser interaction. Specifically, only sets of ions whose absolute summed momenta are less than 30 atomic units (a.u.) in each dimension are considered. Enforcing this momentum conservation constraint strongly reduces the relative contribution from false coincidences, as true coincidences must meet this momentum conservation criteria. Unsurprisingly, under the measurement conditions of a very high number of events per laser shot employed, the three-fold coincidence map (the '$\langle ABC \rangle$' term) in Fig. 1 is heavily dominated by false coincidences, even with momentum conservation applied. This is demonstrated by the similarity of the '$\langle ABC \rangle$' covariance image to the other maps shown in Fig. 1. The covariance analysis routine is therefore crucial to subtract false coincidence contributions to reveal the true correlated ion momenta which are used to probe the Coulomb explosion dynamics. We emphasize, however, that the covariance analysis can be applied without such filtering, as is used extensively in the current work to study the dynamics of three-body fragmentation channels that yield a neutral fragment.

Fluctuating experimental conditions can adversely affect covariance mapping[40,41,50]. For instance, fluctuations in laser intensity, which affect the overall count rate, serve to correlate all ion species[51,52]. This is particularly the case with Self Amplified Spontaneous Emission (SASE) FELs, which are characterized by large amplitude shot-to-shot fluctuations in the total pulse energy. In the present work, this is taken into account using a contingent covariance analysis procedure[53,54]. The total dataset was binned by the single-shot pulse energy recorded by the FLASH GMD, and covariances were computed separately for each pulse energy bin, and then averaged. For this analysis, data for estimated on-target pulse energies between 15.3 and 28.1 $\mu J$ were considered, and separated into 15 bins with equal statistics

### 2. *Coulomb Explosion Simulations*

To aid in the interpretation of the experimental data, a range of classical Coulomb explosion simulations were performed, primarily using the PyCESim Python package[55]. In short, unit charges are placed in positions that reflect a given molecule geometry. The forces acting upon these point charges are determined using Coulomb's law, and their classical trajectories are simulated by numerically solving the resultant second-order differential equations for a series of time points. Non-linear time steps were employed, to allow accurate simulation at early times (in 0.5 fs steps) out to very long times (500 ps), to ensure asymptotic momenta are captured. Sequential fragmentations can be treated by a two-step simulation. In the first step, the metastable diatomic intermediate is treated as a single point charge, and in the second step it dissociates into two species. The dissociation vector of the secondary fragmentation is determined by rotating the diatom in the plane of the molecule, by an angle determined by the secondary dissociation time (sampled considering a specified exponential lifetime) and a classical rotational period. For the Coulomb Explosion simulations presented in Fig. 5, the initial distributions of atomic positions and momenta were accounted for through harmonic Wigner sampling[56–58], as implemented in the PyCESim package[55] and described in detail in the SM (Section S2).

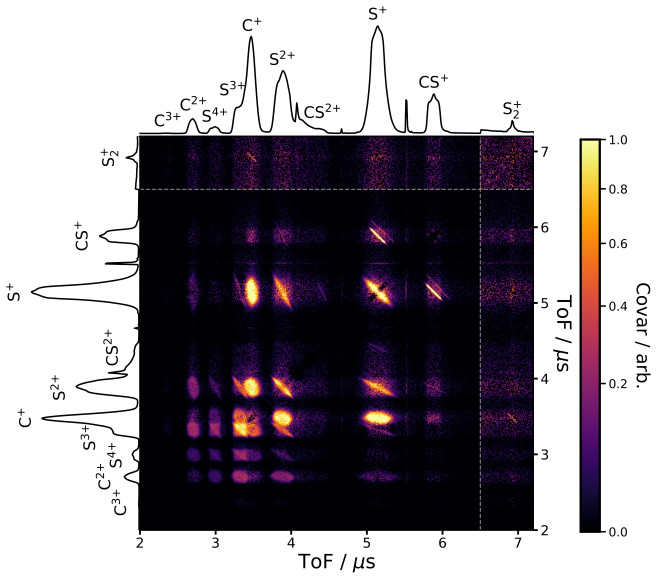


FIG. 2. Time-of-flight covariance map for $CS_2$ ionized in intense soft X-ray pulses at ~180 eV. Labeled one-dimensional ion time-of-flight spectra are projected on the $x$ and $y$ axes. Signal at times-of-flight greater than 6.5 μs (indicated by dashed grey lines) have been multiplied by a factor of 20, to improve the visibility of the weak ($S_2^+$, $C^+$) feature.

## III. RESULTS AND DISCUSSIONS

### A. Observed fragmentation channels

Figure 2 shows the time-of-flight contingent covariance map[45,54] for $CS_2$ subject to intense soft X-ray free-electron laser pulses. This covariance map allows us to identify and isolate pairs of ions produced in the same fragmentation channel, and which are therefore positively correlated. Immediately, a broad range of Coulomb explosion channels can be identified, originating from multiple total charge states of $CS_2$, which fragment predominantly into atomic ions. A detailed discussion of the branching ratios between the different channels considered in the current work is presented in Section III D.

In Fig. 2, signals from two-body Coulomb explosions appear as sharp lines, with negative gradients. This arises simply due to momentum conservation. If one of the two ions produced in the fragmentation has a shorter time-of-flight (because its initial velocity points towards the detector), then the other ion must have a longer time-of-flight (because its initial velocity points away from the detector). By far the most intense two-body feature corresponds to the two-body fragmentation of the $CS^{2+}$ dication into $CS^+$ and $S^+$.

We highlight here the presence of some additional two-body fragmentation channels observed in the covariance map. Firstly, there is a weak signal corresponding to the other possible two-body fragmentation channel of the molecular dication, into $S_2^+ + C^+$. Based on the total covariance signal, and assuming equal detection efficiencies for the relevant ions, we estimate that this channel constitutes ∼0.3% of two-body dication fragmentations. Despite the wealth of previous work on the ionization and fragmentation of $CS_2$, there has been relatively little attention given to this channel, which requires substantial geometric rearrangement and bond formation within the molecular dication. However, there have been several recent studies into the analogous process in the closely related OCS molecule, i.e. dication fragmentation into $SO^+ + C^+$[59–61]. In $CS_2$, the $S_2^+ + C^+$ channel was observed in a coincidence imaging study by Lavollée[20] using synchrotron radiation around the S 2p ionization threshold. However, the channel was not observed in previous or subsequent work covering similar photon energies[19,21]. We note that work by Eland and coworkers using HeII radiation (48.8 eV) studied the $S_2^+ + C^+$ channel, using electron-ion-photon (produced from fluorescence) coincidence techniques. This joint experimental-theoretical study suggested that the $S_2^+ + C^+$ formation occurs from electronically excited $CS_2^{2+}$ with sufficient internal energy in the bending mode[62]. Secondly, weak features arising from two-body fragmentation of the trication into either $S^{2+} + CS^+$ or $S^+ + CS^{2+}$ can be identified. The total kinetic energy release (KER) distributions associated with these processes, extracted through covariance analysis, will be discussed in the following.

Signals arising from three-body fragmentations necessarily yield more diffuse features in the time-of-flight covariance map, as the two correlated ions no longer have opposite momenta of equal magnitude. However, given the near-linear geometry of $CS_2$ prior to explosion, the majority of a concerted explosion's KER is partitioned into $S^{n+}$ ions, which are emitted at relative recoil angles close to 180 degrees. Consequently, $S^{n+}$, $S^{n+}$ correlations appear as diffuse features with negative slopes in Fig. 2. $C^{n+}$, $S^{m+}$ correlations appear as more 'rounded' islands, due to the relative recoil angles close to 90 degrees. The observation of multiply charged atomic ions correlated with one another (including, for instance, the $S^{4+}$, $S^{4+}$ pair) indicates the ability of high total charge states to be reached under our experimental conditions. The photon energy employed lies ∼10 eV above the S 2p binding energy of $CS_2$. Ionizing from this core site has a large cross-section (for instance, the absorption cross-section just above the 2p threshold in Ar is ∼4 MBarn[63]), and a single S 2p ionization event deposits one, two or three total charges on the molecule, with polycation formation involving AM decay(s). Previous measurements at around 180 eV photon energy suggest that $CS_2^{2+}$ is the predominant charge state following single photon absorption (∼70–75%), with $CS_2^+$ and $CS_2^{3+}$ each having ∼10–15% branching ratios[19,64] As the S 2p binding energy is expected to increase substantially in the resultant polycation, we expect that populating the highest total charge states observed in our experiment must involve further (inner-) valence ionizations. In the present manuscript, we focus solely on channels originating from the dication or trication. We believe that under our experimental conditions, both dication and trication formation occur predominantly by a single S 2p ionization followed by one (dication) or two (trication) AM decay(s). A significant contribution to trication formation by valence ionization of dications produced from S 2p ionization and AM decay is excluded based on a power-dependence analysis which is presented in the SM (Section S9).~~, which are predominantly populated by a single S 2p ionization and AM decay(s)~~. As noted earlier, data relating to higher charge states, formed through multiple photoabsorption events, will be presented in a separate publication[27].

### B. Two-body Fragmentation Dynamics

Using covariance analysis, the total KER distributions for each observed two-body fragmentation channel were extracted, and are plotted in Fig. 3. These are compared with predictions from Coulomb's law for two charges separated by one and two times the equilibrium C-S bond distance, $r_{CS}$. It can be seen that the two channels originating from the molecular dication have broadly similar distributions, peaking at around 5 eV, close to that predicted for two single charges repelling from a distance of $2r_{CS}$. The rearrangement channel, $S_2^+ + C^+$, however, peaks at slightly lower values, with a less pronounced tail toward higher KERs. The observed KER distributions are similar to those previously reported for the $S^+ + CS^+$ channel prompted by electron impact ionization by Wang *et al.*[13], albeit peaking at slightly higher energies. The mean KER for the $S^+ + CS^+$ channel, 6.00 eV, agrees rather well with that reported by Saha *et al.* using synchrotron ra-

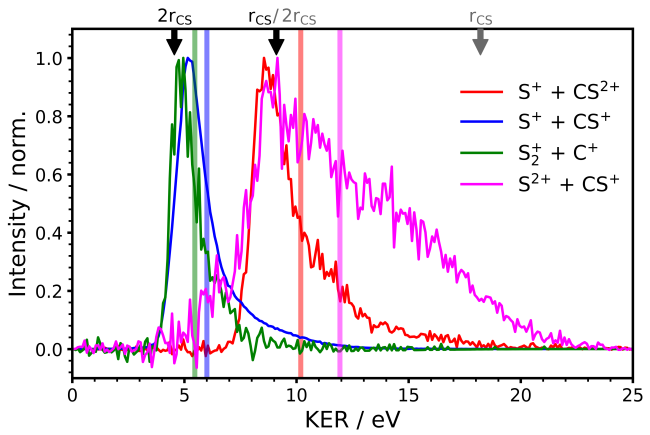


FIG. 3. Kinetic energy release (KER) distributions extracted through covariance analysis for the observed two-body fragmentation channels. Predicted KERs using Coulomb's law for two charges separated at distances related to the equilibrium bond distances for $CS_2$ are indicated by the black (dication) and gray (trication) arrows. The mean of each KER distribution is marked with colored vertical lines.

diation with a 171 eV photon energy[21]. Saha *et al.* reported mean KERs of 5.0, 5.8 and 6.4 eV for fragmentations formed in conjunction with AM electrons in different kinetic energy regions. As mentioned previously, Lavollée observed the $S_2^+$+ $C^+$ channel following excitation around the S 2p ionization threshold[20]. Their measured KER distribution peaked at very similar energies to the $S^+$+ $CS^+$ channel, with the $S_2^+$+ $C^+$ channel exhibiting a slightly narrower KER distribution, in agreement with our results. We do, however, note that their KER distributions peak at slightly lower values (∼4.5 eV), and that they observe a low energy shoulder at 1 eV for the $S_2^+$+ $C^+$ channel, which is absent in the current work, and may have arisen from false coincidences.

The potential energy curves of the $CS_2^{2+}$ dication have been previously computed and examined by Hochlaf *et al.*[65]. As implied by the observation of $CS_2^{2+}$ in the time-of-flight spectrum (at ∼5.55µs, see Fig. 2), the ground state of the dication is stable. There are, however, multiple low-lying electronic states whose vertical population would result in a KER of around 5 eV. In the theoretical work of Hochlaf *et al.*[65], only dissociation to the $S^+$+ $CS^+$ products was considered. Future theoretical work considering the possible paths to formation of $S_2^+$+ $C^+$ would be of great interest[62].

The shapes of the KER distributions for the pair of two-body trication fragmentation channels again agree well with those reported by Wang *et al.*[13], with our KERs being again slightly higher than those reported previously. The two channels peak at similar KERs (∼9 eV), slightly lower than that predicted by Coulomb's law for a separation of $2r_{CS}$. However, the two channels exhibit very different KER distributions, with the $S^{2+}$+ $CS^+$ channel exhibiting a very broad tail up to high KERs, as well as a small shoulder at lower KERs. Lavollée observed qualitatively similar KER distributions for the two-body trication fragmentation channels[20], although both the high KER tail and low KER shoulder in the $S^{2+}$+ $CS^+$ channel are less prominent than in the current data. This low KER shoulder overlaps with the KER distributions of the dication fragmentations. Speculatively, the low KER signal observed could arise from a dication fragmentation which leads the $S^+$ fragment in some highly excited autoionizing state, leading ultimately to $S^{2+}$ once the separation from the $CS^+$ is large. The very broad KER distribution of the $S^{2+}$+ $CS^+$ channel is intriguing and may point to the population of a broad range of excited electronic states of $CS_2^{3+}$ which correlate to this dissociation limit.

### C. Three-body Fragmentation Dynamics

#### 1. *The* $S^+$+ $C^+$+ $S^+$ *Channel*

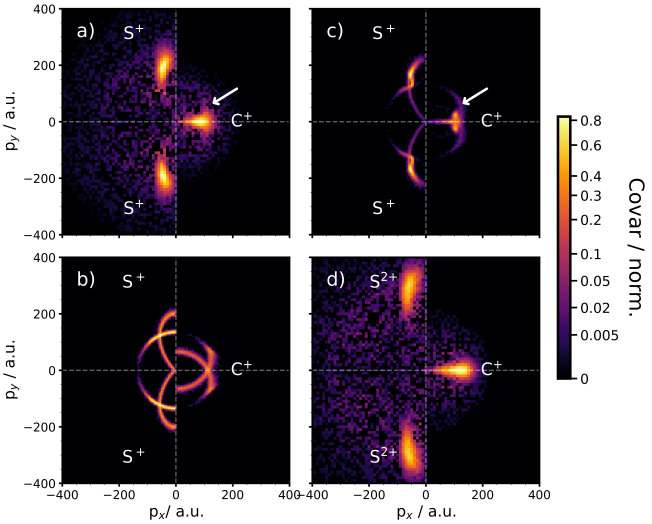


FIG. 4. a) Experimental Newton plot for the ($S^+$, $C^+$, $S^+$) channel. Weak features in the $C^+$ momentum distribution, appearing as a roughly vertical line, are highlighted with an arrow. b) Simulated Newton plot for the ($S^+$, $C^+$, $S^+$) channel, for a fully sequential dissociation, as described in the text. c) Simulated Newton plot for the ($S^+$, $C^+$, $S^+$) channel, for a fast sequential/asynchronous dissociation, as described in the text. d) Experimental ($S^{2+}$, $C^+$, $S^{2+}$) Newton plot, as example signal for a fragmentation of a higher total charge state.

Figure 4a) shows the covariant Newton plot for the ($S^+$, $C^+$, $S^+$) channel, which is computed by enforcing momentum conservation (see discussion in Section II B 1). Here the *x* axis is defined by the bisector of the two $S^+$ momenta, and the ion momenta are plotted within the *xy* plane. The primary feature shows $S^+$ ions recoiling at close to 180 degrees from each other, with the $C^+$ emitted with relatively low momenta at close to 90 degrees. Compared to previous work studying $CS_2$ in intense laser fields[16,18], one significant difference is the lack of a signal clearly assignable to a sequential fragmentation. Such a channel would produce arcing features in the Newton plot, due to the lack of angular correlation between the recoil vectors of the first and second steps. In pre-

vious work employing strong-field ionization, such a channel made a significant contribution. For instance, in the work of Hishikawa *et al.*[16] (800 nm, 60 fs, $0.36 \times 10^{15}$ Wcm$^{-2}$), 17% of $S^+$+ $C^+$+ $S^+$ dissociations were determined to occur through sequential breakup via a $CS^{2+}$ intermediate. Synchrotron radiation studies by Guillemin *et al.*[22,23] employing S 1s core ionization have examined the interplay between concerted and sequential breakup from $CS_2^{4+}$ to yield $S^{2+}$+ $C^+$+ $S^+$, again via a $CS^{2+}$ intermediate. This sequential dissociation was found to be responsible for 7% of the coincidence counts in this channel.

Figure 4b) shows a classical Coulomb explosion simulation for such a sequential fragmentation. In this simulation, the initial dissociation into $CS^{2+}$ + $S^+$ is treated as two classically repelling point charges. For each simulation, a time at which the secondary $CS^{2+}$ fragmentation occurs is sampled based on an exponential lifetime of the intermediate. The first step of the simulation is run until this time, after which the C and S atoms are rotated by an angle determined by the ratio between the time of the secondary dissociation and a rotational period of the $CS^{2+}$. A classical simulation of the secondary fragmentation is then launched from this geometry, retaining the atomic velocities of the initial simulation. In the SM Fig. S7, we show a sequence of Newton plots for different input parameters to the simulation. For the plot shown in Fig. 4b), a lifetime much greater than that of the rotational period was chosen (i.e. a truly sequential fragmentation), leading to the extensive arcing features in the Newton plot.

Weak features partially resembling that expected for a sequential fragmentation are visible, particularly in the form of "fins" on the main $C^+$ feature, with greater $|\, p_y \,|$ in the Newton frame. These features do not fully extend around the Newton plot, as would be expected for a completely sequential process. This signal is difficult to see without a non-linear color scale, such as that employed in Fig. 4, and its magnitude is close to that of the noise in the experimental covariance image. However, these signals may be explained by a fast sequential, or asynchronous, breakup. This is explored in panel c), which repeats the sequential simulation but now assumes a much shorter $CS^{2+}$ lifetime. For the data shown in panel c) a lifetime of 50 fs and a rotational period of 400 fs was assumed. Qualitatively, this does resemble the weak experimental signals identified. As for why no clear signal associated with long-lived sequential fragmentation is identified, it is difficult to say conclusively whether this is because the trication is populated in a different way from previous work (S 2p ionization as opposed to strong-field ionization[16]), or due to a lack of sufficient signal-to-noise in this covariance image. In the SM, we present additional representations of the ($S^+$+ $S^+$+ $C^+$) covariance (Figs. S5 and S6), which again show no clear indications for a truly sequential breakup. For fragmentations originating from higher charge states, no features clearly assignable to asynchronous breakup can be identified in the Newton plots, as in the example ($S^{2+}$, $C^+$, $S^{2+}$) case shown in Fig. 4d).

Figure 5a) shows the experimental ($S^+$, $C^+$, $S^+$) three-fold covariance as a function of the total KER and the recoil angle between the two $S^+$ ions, $\beta(S^+, S^+)$. This is compared with simulated data assuming the instantaneous charge-up and classical repulsion of an ensemble of $CS_2$ molecules, with starting atomic ion positions and velocities sampled from a Wigner distribution (as described in detail in the SM Section S2). To further enable comparison between the two, panels c) and d) present projections over the $\beta$ and KER axes, respectively. It can be seen that the mean KER of the $S^+$ + $C^+$ + $S^+$ explosion is well reproduced by the simulation. However, the simulation predicts a very narrow KER distribution, while that observed experimentally is much broader (∼10 eV full width at half maximum). This can be related to several factors not included in the simple simulations, such as deviations of the relevant trication potential from a purely Coulombic potential, participation of multiple electronic states in the fragmentation, nuclear dynamics on the cation and dication states and the potential role of charge transfer processes. The agreement in the breadth of the $\beta$ distribution is much better, albeit with the experimental distribution slightly broadened and shifted to more acute angles relative to the simulation. Still, this comparison indicates that the recoil angular distribution is largely accounted for by Wigner sampling the spread of initial atomic positions and momenta, particularly along the degenerate bending modes. This implies that bending motion initiated by X-ray ionization prior to dissociation is fairly minimal, in direct contrast to previous experimental results in intense NIR fields, where substantial bending en route to dissociation was observed, leading to more acute recoil angles[15,17].

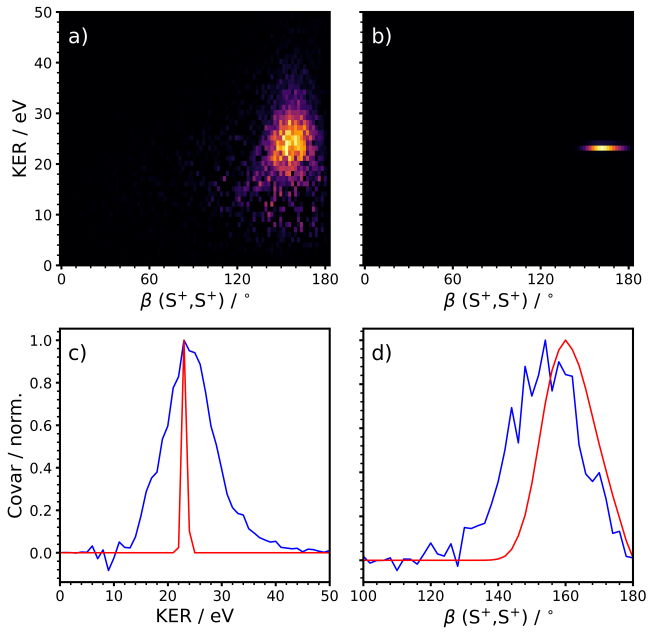


FIG. 5. a) Experimental and b) simulated ($S^+$, $C^+$, $S^+$) covariance signals as a function of $\beta$ ($S^+$, $S^+$), the relative recoil angle of the two $S^+$ ions, and the total KER. Panels c) and d) compare one-dimensional KER and $\beta$ distributions from the experiment (blue) and simulation (red).

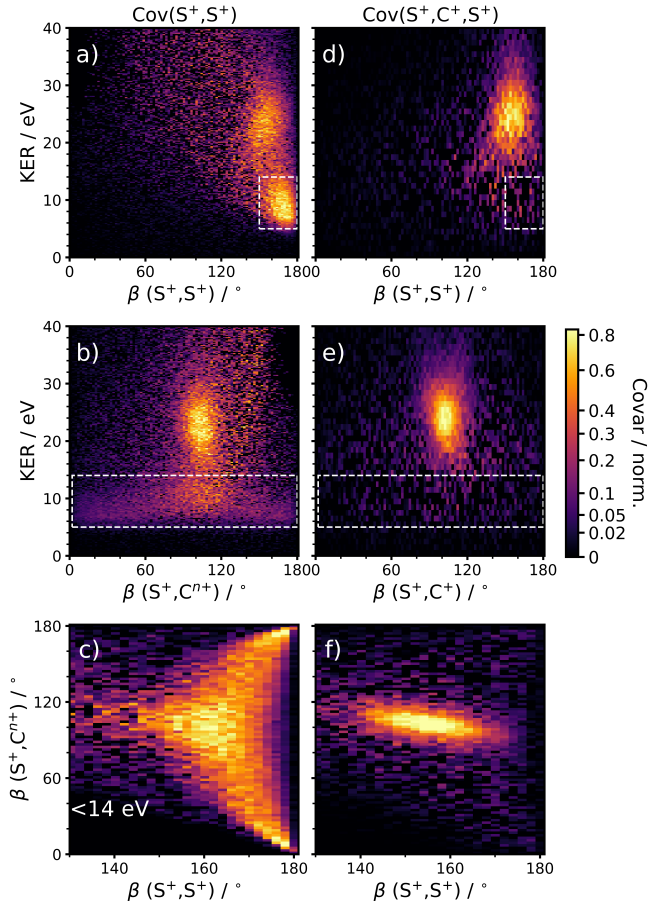


FIG. 6. Two-fold ($S^+$, $S^+$) covariance (a) to c)), and three-fold ($S^+$, $C^+$, $S^+$) covariance (d) to f)). Correlations are shown between: the total KER, the recoil angle between the two $S^+$ atoms and the $S^+$ ions and the third fragment. In the two-fold covariance, this momentum is inferred from momentum conservation, while in the three-fold case it is measured, and solely arises from $C^+$ ions. In panel c), signal is only plotted for total KERs less than 14 eV, to isolate signal from the dication fragmentation channel, which is highlighted with a white box in other panels. As discussed in the main text, such signal is absent in the three-fold covariance.

### 2. *The* $S^+ + C + S^+$ *and* $S^+ + C^+ + S$ *Channels*

Our experiment is also sensitive to three-body fragmentations which yield a neutral fragment. For the $CS_2^{2+}$ dication this generates either $S^+ + C + S^+$ or $S^+ + C^+ + S$, and both channels are observed. Much of the past work on $CS_2$ has neglected these channels, although they are fairly prominent dication fragmentation channels. This may be because these channels are more challenging to analyze in traditional coincidence experiments. Due to the undetected neutral fragment with non-zero momentum, contributions from false coincidences cannot be filtered out by enforcing momentum conservation constraints. Therefore, coincidence measurements involving neutral fragments need to be carried out at even lower count rates, to ensure that false coincidences can be neglected. Both channels were studied by Lablanquie *et al.*, induced by single-photon double ionization in the vacuum ultraviolet[25], however, the mechanistic insights, such as whether dissociation occurs via a concerted or sequential pathway, were limited due to the inability to record (relative) three dimensional ion momenta. Eland also studied these dissociation pathways following single-photon vacuum ultraviolet double ionization using HeII radiation[66] and coincidence time-of-flight mass spectrometry. Based on the slopes of coincident ion pairs (for both $CS_2$ and the closely related OCS), for the $S^+ + C^+ + S$ fragmentation channel, Eland could not distinguish between a concerted mechanism, and a sequential fragmentation involving a very low KER $CS^+$ breakup into $C + S^+$. A conclusive assignment could also not be made for the $S^+ + C + S^+$ channel, with Eland stating that on the basis of the data, a sequential fragmentation seemed unlikely, but could not be eliminated. Saha *et al.* studied these channels in more detail following 171 eV photoabsorption, and reported relative ion momenta of the species involved[21]. From an analysis based on Newton plots and Dalitz plots, they concluded that fragmentation was concerted in both channels, with $S^+ + C^+ + S$ predominantly originating from bent and asymmetrically stretched configurations, with the $S^+ + C + S^+$ fragmentation occurring from any geometry. Plots of our covariance data in the same Dalitz plot representation used in this prior work are shown in the SM (Fig. S13). As discussed shortly, our native frames analysis leads to a different interpretation for the mechanism underlying the $S^+ + C + S^+$ channel. This analysis points to the coexistence of sequential and concerted fragmentation mechanisms for this channel.

Two-fold covariance analysis allows these fragmentation channels with a neutral cofragment to be studied without contamination from false coincidences. Figures 6a)-c) present a two-fold ($S^+$, $S^+$) covariance analysis. Here, the momentum of the third, undetected fragment (which may be a neutral C or charged $C^{n+}$ ion) is defined as the negative of the sum of the two $S^+$ ions, such that the total momentum of the three particles is zero. The intensity is then plotted as a function of the total KER (including the KER of the inferred third particle), the angle between the two $S^+$ momenta and the angle between the $S^+$ and $C^{0/n+}$ momenta. Two prominent features are observed. The first occurs with a KER of ∼20–30 eV and a well-defined angle between the $S^+$ and $C^{0/n+}$ of around 100°. This arises from the three-body Coulomb explosion of the trication into $S^+ + C^+ + S^+$.

A second channel with a significantly lower KER of ∼6–14 eV is also seen, and is highlighted. This arises from fragmentations of the dication to produce $S^+ + C + S^+$. This can be confirmed by comparing to the analogous three-fold ($S^+$, $C^+$, $S^+$) covariance, shown in Fig. 6 panels d)–f), in which this island of signal is absent. A carefully-weighted subtraction of the three-fold covariant KER distribution from that of the two-fold covariance can extract the KER distribution associated with the dication fragmentation feature, showing that the higher-energy dication fragmentations do overlap in KER with lower-energy trication fragmentations (Fig. 10). In the current analysis we focus on the range of KERs for which the two distributions do not overlap.

For the $S^+$+ C + $S^+$ channel, the two $S^+$ ions are emitted at close to 180 degrees from one another, whereas the angle between $S^+$ and C can take a wide range of angles, with the highest intensity localized around 100 degrees, similar to the maximum in the $S^+$+ $C^+$+ $S^+$ Coulomb explosion. In principle, this three-body dication fragmentation can arise from either a concerted fragmentation or a sequential process via a $CS^+$ intermediate. The observation of a broad $\beta(S^+, C)$ distribution with a peak in intensity close to that of the concerted trication fragmentation may indicate that both pathways contribute.

To explore the contributions from sequential and concerted dissociation pathways further, we turn to a native frames analysis, as recently applied in a number of studies into three-body fragmentation dynamics[28–30,67,68]. Put simply, this method involves analyzing the two steps of a sequential fragmentation in different coordinate frames, native to each fragmentation step. This can allow the clear distinction between sequential and concerted fragmentation, and enable extraction of physical properties such as the KER distributions associated with each step of a sequential breakup. This analysis, which is described in detail in the SM Section S3, yields the KERs associated with the primary and secondary fragmentations, $\mathrm{KER}_{\mathrm{CS}^+_{\mathrm{II}},\mathrm{S}^+_{\mathrm{I}}}$ and $\mathrm{KER}_{\mathrm{CS}^+_{\mathrm{II}}}$ as well as the angle between the two dissociation vectors, $\theta_{\mathrm{CS}^+_{\mathrm{II}},\mathrm{S}^+_{\mathrm{I}}}$.

For a truly sequential fragmentation (where the lifetime of the $CS^+$ intermediate is much longer than its rotational lifetime), we would expect the signal to appear uniformly distributed over $\theta_{\mathrm{CS}^+_{\mathrm{II}},\mathrm{S}^+_{\mathrm{I}}}$ (i.e. there is no correlation between the direction of the primary and secondary dissociation events), and for the KERs to be independent of $\theta_{\mathrm{CS}^+_{\mathrm{II}},\mathrm{S}^+_{\mathrm{I}}}$. Furthermore, we should expect that $\mathrm{KER}_{\mathrm{CS}^+_{\mathrm{II}},\mathrm{S}^+_{\mathrm{I}}}$ is significantly greater than $\mathrm{KER}_{\mathrm{CS}^+_{\mathrm{II}}}$, as the former KER is associated with a Coulomb explosion of a dication, and the latter a dissociation of a monocation.

Figure 7 displays the ($S^+$, $S^+$) covariance as a function of these native frame quantities. The signal is plotted for total KERs of less than 12 eV, to isolate signal from the $S^+$+ $C^+$+ $S^+$ channel. Firstly, in panel a), covariance is plotted as a function of $\mathrm{KER}_{\mathrm{CS}^+_{\mathrm{II}}}$ and $\theta_{\mathrm{CS}^+_{\mathrm{II}},\mathrm{S}^+_{\mathrm{I}}}$. The most intense signal is found with a broad range of KER and $\theta_{\mathrm{CS}^+_{\mathrm{II}},\mathrm{S}^+_{\mathrm{I}}} \gtrsim 120°$, which we will return to shortly. In addition to this, there is a feature with very low $\mathrm{KER}_{\mathrm{CS}^+_{\mathrm{II}}}$, marked with a green rectangle, that appears to span all angles (although it heavily overlaps other features at larger $\theta_{\mathrm{CS}^+_{\mathrm{II}},\mathrm{S}^+_{\mathrm{I}}}$). As mentioned above, this is expected for a sequential fragmentation, in which the dissociation vector of the secondary fragmentation is isotropic with respect to the initial dissociation velocity. Panel b) presents covariance as a function of $\mathrm{KER}_{\mathrm{CS}^+_{\mathrm{II}},\mathrm{S}^+_{\mathrm{I}}}$ and $\theta_{\mathrm{CS}^+_{\mathrm{II}},\mathrm{S}^+_{\mathrm{I}}}$, for $\mathrm{KER}_{\mathrm{CS}^+_{\mathrm{II}}} < 1$ eV, to isolate sequential fragmentation signal. Again, as expected, $\mathrm{KER}_{\mathrm{CS}^+_{\mathrm{II}},\mathrm{S}^+_{\mathrm{I}}}$ spans all $\theta_{\mathrm{CS}^+_{\mathrm{II}},\mathrm{S}^+_{\mathrm{I}}}$, and the KER distribution is independent of $\theta_{\mathrm{CS}^+_{\mathrm{II}},\mathrm{S}^+_{\mathrm{I}}}$. From these covariances, we can extract the KER distributions associated with the two steps of the sequential fragmentation, as shown in panel c). This was done by summing over the appropriate axis for $\theta_{\mathrm{CS}^+_{\mathrm{II}},\mathrm{S}^+_{\mathrm{I}}} < 60°$. It is interesting to note that the KER associated with the initial fragmentation step into $S^+$+ $CS^+$ peaks at around 7–8 eV. This is significantly higher than that observed for the $CS^+$+ $S^+$ channel, which peaks close to 5 eV (see Fig. 3). This observation, which is consistent with the KER distribution reported by Saha *et al.*[21], suggests that it is the higher KER $CS^+$+ $S^+$ fragmentations which produce sufficiently energetic $CS^+$ ions to undergo this secondary dissociation.

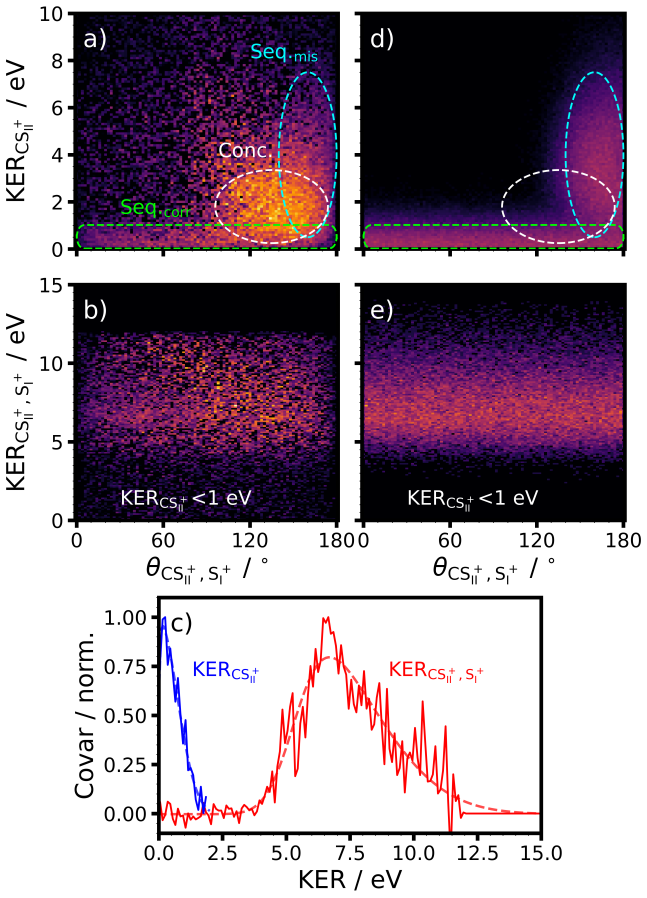


FIG. 7. Native frame covariance analysis for the ($S^+$, $S^+$) ion pair. Panels a) and b) plot experimental covariance intensity as a function of $\theta_{\mathrm{CS}^+_{\mathrm{II}},\mathrm{S}^+_{\mathrm{I}}}$ and $\mathrm{KER}_{\mathrm{CS}^+_{\mathrm{II}}}$ (a) and $\mathrm{KER}_{\mathrm{CS}^+_{\mathrm{II}},\mathrm{S}^+_{\mathrm{I}}}$ (b). In b), signal is displayed only for $\mathrm{KER}_{\mathrm{CS}^+_{\mathrm{II}}} < 1$ eV. Panel c) displays the KER distributions extracted from the data shown in panels a) and b) by integrating over $0 < \theta_{\mathrm{CS}^+_{\mathrm{II}},\mathrm{S}^+_{\mathrm{I}}} < 60°$. Panels d) and e) display the output of sequential fragmentation simulations plotted in the same manners as a) and b), respectively. In panels a) and d), regions of interest are marked according to their assigned predominant origin (discussed in detail in the main text): sequential fragmentation in which $S^+_I$ is correctly assigned (green), sequential fragmentation in which $S^+_I$ is misassigned (cyan) and concerted fragmentation (white).

Our assignment of this sequential fragmentation can be supported by simple simulations. Here, the KER distributions associated with the primary and secondary fragmentations were

extracted from the experimental data shown in Figure 7c) by fitting the distributions to a skewed normal distribution. The KER distributions associated with each step were then randomly sampled. The dissociation vector of the secondary $CS^+$ fragmentation was randomly rotated around the fragmentation plane, and the final momenta of each particle computed. Panels d) and e) show simulated data processed in an analogous way to the experimental data. As expected, agreement with the experiment is strong, within the experimental signal-to-noise. In the simulation, an island of signal is seen to span a range of $KER_{CS_{II}^+}$ for $\theta_{CS_{II}^+,S_I^+} < 120^\circ$, as indicated with a cyan ellipse in Fig. 7. This arises because in the data analysis, $S_I^+$ and $S_{II}^+$ are not distinguished, and so in 50% of cases, the 'wrong' $S^+$ ion is assigned as $S_I^+$[67]. In the simulation, the two $S^+$ ions can be distinguished, and if this is done, this signal is absent, as shown in the SM (Fig. S8) and as discussed previously in the literature[67].

The simulated data shown in 7d) for a purely sequential fragmentation fails to capture the intense experimental signal that spans $\theta_{CS_{II}^+,S_I^+} > 120^\circ$ and $KER_{CS_{II}^+}$ ~0–4 eV, highlighted by the white ellipse in Fig. 7 . This signal is assigned to (near) concerted fragmentation into $S^+ + C + S^+$. This assignment is supported by native frames analysis of simple simulations of the concerted fragmentation, as shown in the SM (Fig. S9). An accurate modeling of this concerted breakup would ideally involve trajectory calculations on the relevant electronic states of the $CS_2^{2+}$ dication, which is out of the scope of the current work. The approximate total KER distributions for this process, as well as recoil angle distributions, can be seen by comparing the covariances shown in Fig. 6 to the analogous analysis for the sequential fragmentation simulations. This is done in SM Fig. S11. It can be seen that the KER distribution associated with the concerted fragmentation spans slightly higher energies than that of the sequential dissociation. Similar to the concerted trication breakup into $S^+ + C^+ + S^+$, the $S^+$ and $C^+$ recoil at around 100° from one another.

The other possible three-body dication fragmentation channel, which produces $S^+ + C^+ + S$, can be studied by considering correlations between $C^+$ and $S^+$ ions, as shown in Fig. 8. Once more, signal can be identified in the < 14 eV KER region which is absent in the three-fold ($S^+$, $C^+$, $S^+$) covariance, and can therefore be assigned to this three-body dication fragmentation channel. Once more, there is however some overlap in the KER distributions from the dication and trication fragmentations, as discussed shortly in relation to Fig. 10. The dication fragmentation signal is associated with $S^+$, $S^+$ recoil angles close to 180°, while the $S^+$, $C^+$ recoil angle spans a range of angles >100°. As shown in the SM Fig. S12, performing native frames covariance analysis on this feature suggests that the fragmentation does not occur truly sequentially via a long-lived intermediate. Instead, the broad range of $S^+$, $C^+$ recoil angles can be understood in terms of nuclear motion of the $CS_2^{2+}$ dication prior to dissociation and/or an asynchronous nature to the breakup, as previously suggested by Saha *et al.*[21].

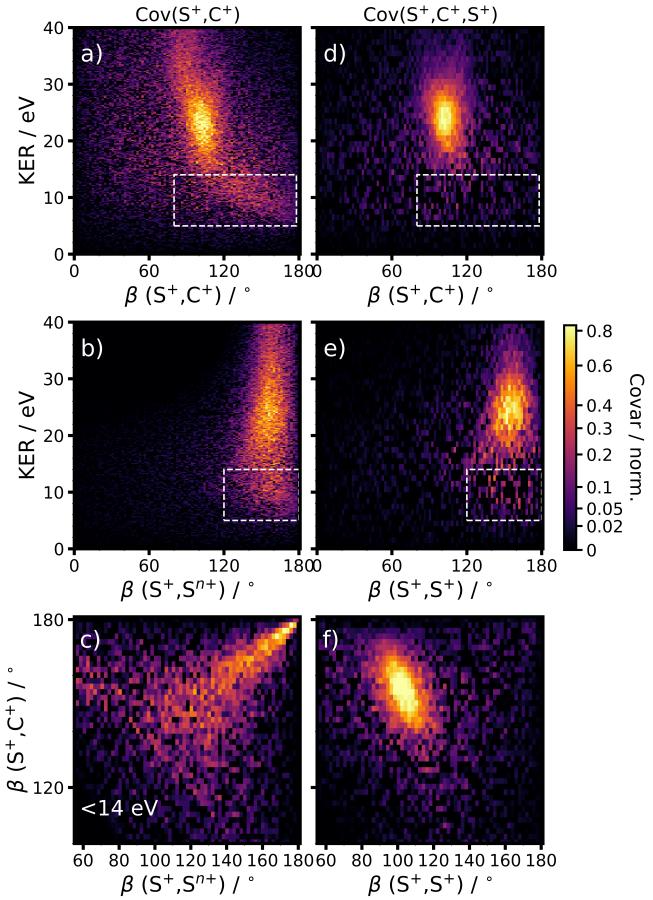


FIG. 8. Two-fold ($S^+$, $C^+$) covariance (a) to c)), and three-fold ($S^+$, $C^+$, $S^+$) covariance (d) to f)). Correlations are shown between: the total KER, the recoil angle between the two $S^{n+}$ atoms and the $S^+$ ion and the $C^+$. In the two-fold covariance, the momentum of the third ion ($S^{n+}$) is inferred from momentum conservation, while in the three-fold case it is measured, and solely arises from $S^+$ ions. In panel c), signal is only plotted for total KERs less than 14 eV, to isolate signal from the dication fragmentation channel, which is highlighted with a white box in other panels. As discussed in the main text, such signal is absent in the three-fold covariance.

### 3. *The* $S^{2+} + C + S^+$ *and* $S^{2+} + C^+ + S$ *Channels*

Dissociations of $CS_2^{3+}$ trications that yield neutral fragments and an asymmetric distribution of charges among atomic fragments are also possible. Again, these have received limited attention in ion imaging studies, but have been observed with coincidence time-of-flight techniques. Using 180 eV synchrotron radiation, Eland *et al.* reported that trications fragmenting into the $S^{2+} + C^+ + S$ and $S^{2+} + C + S^+$ channels had branching ratios of 24% and 29%, respectively[64]. Contrastingly, only the latter channel was observed at 180 eV by Ankerhold *et al.*[19], occurring for roughly 13% of triple ionizations. These channels can be studied using correlations between $S^{2+}$ and $C^+$ ions, and between $S^{2+}$ and $S^+$ ions, respectively.

Fig. 9 shows $\beta$ KER representations of the ($S^{2+}$, $S^+$) two-

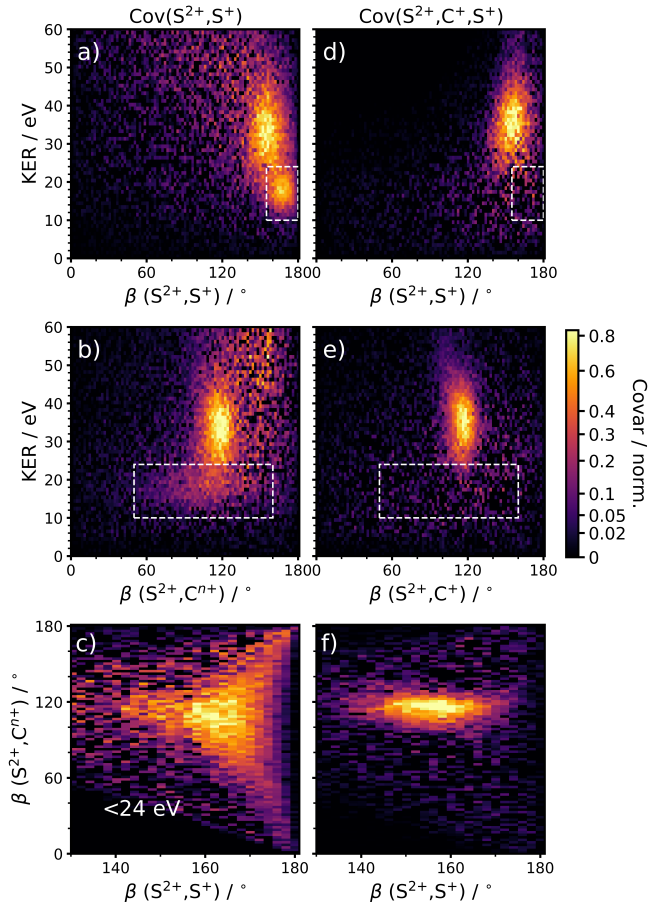


FIG. 9. Two-fold ($S^{2+}$, $S^+$) covariance, experimental (a) to c)), and three-fold ($S^{2+}$, $C^+$, $S^+$) covariance (d) to f)). Correlations are shown between: the total KER, the ($S^{2+}$, $S^+$) recoil angle and the recoil angle between the $S^{2+}$ ion and the third body. In the two-fold covariance, this particle's momentum is inferred from momentum conservation, whilst in the three-fold case, the $C^+$ momentum is recorded directly. In panel c), signal is only plotted for total KERs less than 24 eV, to isolate signal from the trication fragmentation channel, which is highlighted with a white box in other panels. As discussed in the main text, such signal is absent in the three-fold covariance.

fold covariances, alongside the ($S^{2+}$, $C^+$, $S^+$) three-fold covariance represented in the same manner. The signal with relatively low KER (∼10–24 eV) which is present in the two-fold covariance but absent in the three-fold covariance, can be assigned to the $S^{2+}$+ C + $S^+$ product channel. Compared to the $S^+$+ C + $S^+$ signal in Figure 6, this signal is more localized in $\beta(S^{(2/1)+},C)$, suggesting a greater relative contribution from concerted breakups. This can be confirmed by performing an analogous native frame analysis to that described previously and presented in Fig. S15 of the SM.

A sequential fragmentation yielding $S^{2+}$+ C + $S^+$ could potentially occur via two pathways. In the first pathway, $CS_2^{3+}$ Coulomb explodes into $S^{2+}$ and $CS^+$, with the latter dissociating into C + $S^+$ at later times. In the other pathway, $CS_2^{3+}$ would Coulomb explode into $S^+$ and $CS^{2+}$, which subsequently dissociates into C + $S^{2+}$. While such a charge-asymmetric dissociation may be unfavorable for the dication, such processes are possible[69]. Figure S15 in the SM presents native frame covariances for each of these possible scenarios (i.e. fragmentation via $CS^+$ or $CS^{2+}$). If a sequential pathway were in operation, one would expect features that span all angles at a constant KER. We would also expect that the primary dissociation would have a relatively large KER as it corresponds to a Coulomb explosion between two charged ions, while the secondary dissociation would have a much lower KER. No such signal is observed in either case, and the signal is instead localized to a particular range of angles. We therefore conclude that this channel is dominated by concerted fragmentation.

We also observe signal arising from fragmentation of the parent trication into $S^{2+}$+ $C^+$+ S, revealed by comparing two-fold ($S^{2+}$, $C^+$) covariances to three-fold ($S^{2+}$, $C^+$, $S^+$) covariances (shown in the SM Fig. S14. Native frames analysis again suggests that this channel proceeds in a concerted manner, rather than sequentially via some long-lived intermediate (SM Fig. S16).

### D. Branching Ratios for Dication and Trication Fragmentation Channels

As the total covariance signal associated with a channel is proportional to the frequency with which that specific fragmentation pathway occurs[54], we can assign relative branching ratios for the observed dication and trication fragmentation pathways. Comparison of the intensity of a two-fold covariance to a three-fold covariance can be challenging because the signal intensity associated with the three-fold covariance is lowered by the finite detection efficiency of the third ion. For the three-body fragmentation channels, we therefore estimate the total covariance signal associated with each channel by using a scaled subtraction of the contributing three-fold covariances to decompose the two-fold KER distribution and extract the contribution from each contributing fragmentation channel. In addition to providing a reliable branching ratio determination, this allows the extraction of these KERs, which are otherwise overlapped by three-charge fragmentation channels. This KER decomposition process is shown in Fig 10.

These branching ratios are given in Table I and are compared to literature measurements at 180 eV. Note that here we are not considering any channels which only produce one charged fragment (e.g., $CS_2^+$ into $S^{2+}$ + C + S). The covariance signal for a pair of ions also depends on the detection efficiencies of each ion, but for the current analysis we will assume an equal detection efficiency of all ions. Based on the scaling factors used for subtracting the three-fold covariance KER distributions in Fig. 10, we do not see evidence for a large variation in the detection efficiency across these ions (which lie in the ∼15–25% range). We do note that this variation in detection efficiency will introduce some systematic uncertainty in the extracted branching ratios. Likewise, these branching ratios will have some (gen-

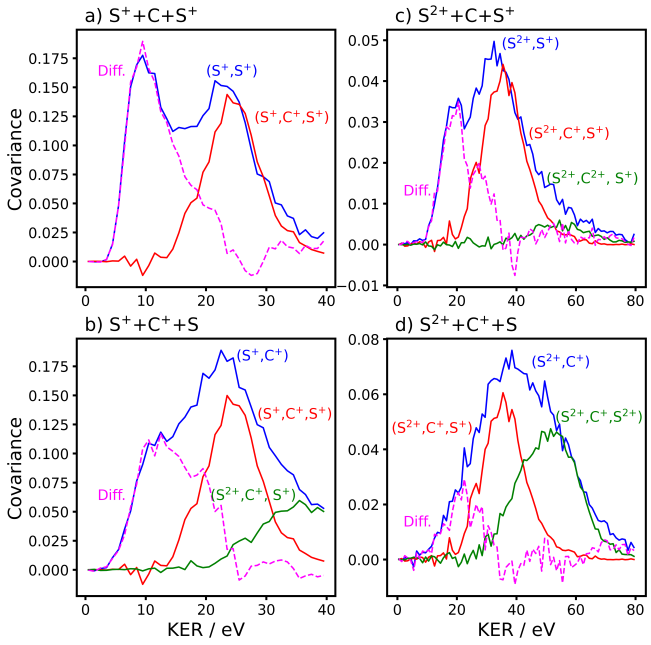


FIG. 10. Extracting the KER distributions for dication and trication fragmentation channels which yield a neutral atomic product, for channels: $S^+ + C + S^+$ (a), $S^+ + C^+ + S$ (b), $S^{2+} + C + S^+$ (c) and $S^{2+} + C^+ + S$ (d). This is done by taking the KER distribution for the relevant two-fold covariance (blue solid lines), and subtracting scaled three-fold covariances (red and green solid lines), to isolate signal associated with the channel of interest (dashed magenta lines). These subtracted KER distributions are then integrated over to determine total covariance signals and therefore branching ratios.

erally smaller) statistical uncertainty that could be in principle be estimated by bootstrapping or knifejacking during the covariance calculations[26,44]. As a result of the very high count rate employed in the current work, computing a given covariance is rather computationally-demanding and so these schemes would require significant computation time and have not been performed. However, a lack of quantitative statistical uncertainty analysis does not preclude the current analysis, which focuses on the general relative frequency of fragmentation channels.

Turning firstly to the dication fragmentation, we can see that in our analysis, the three major breakup channels occur with fairly similar propensity, with $S^+ + C + S^+$ being the most common (40%). The rearrangement channel to yield $S_2^+ + C^+$ is very minor, and accounts for only ∼0.1% of double ionization Coulomb explosion signal. Although Ankerhold *et al.* observed the same three major channels, and all were fairly prominent, they assigned the two-body $S^+ + CS^+$ channel as the dominant channel[19]. As the authors of both papers mention[19,64], there are various systematic errors in quantitatively assigning these branching ratios, such as the assumption of equal detection efficiency of all events. In time-of-flight mass spectrometry measurements, which do not directly record the three-dimensional momentum vector of each ion, decomposing overlapping channels can also be challenging,

| Dication | | | | |
|---|---|---|---|---|
| Channel | Covariance | Ratio | Ratio[19] | Ratio[64] |
| $S^+ + C + S^+$ | 1.92 | 40% | 23.8% | - |
| $S^+ + C^+ + S$ | 1.47 | 31% | 19.2% | - |
| $S^+ + CS^+$ | 1.40 | 29% | 56.9% | - |
| $S_2^+ + C^+$ | 0.00599 | 0.1% | - | - |
| Trication | | | | |
| $S^+ + C^+ + S^+$ | 1.68 | 64% | 86.7% | 29.4% |
| $S^{2+} + C + S^+$ | 0.517 | 20% | 13.3% | 31.6% |
| $S^+ + CS^{2+}$ | 0.0319 | 1.2% | - | 5.4% |
| $S^{2+} + CS^+$ | 0.0466 | 1.8% | - | 7.5% |
| $S^{2+} + C^+ + S$ | 0.365 | 14% | - | 26.1% |

TABLE I. Channel-resolved covariances and branching ratios for fragmentation channels of $CS_2^{2+}$ and $CS_2^{3+}$ which produce two or more charged species. Values are compared to literature reports at 180 eV recorded with synchrotron radiation by Ankerhold *et al.* and Eland *et al.*[19,64]. The values from these literature works have been scaled to reflect branching ratios solely for channels which produced two or more charged species.

and it is difficult to account accurately for the dependence of ion collection efficiency on ion kinetic energy.

Based on our analysis, trications are dominated by the three-body fragmentation into $S^+ + C^+ + S^+$ (64%), with the second most prominent channel being $S^{2+} + C + S^+$ (20%). This is in reasonable agreement with the work of Ankerhold *et al.*[19], although the authors did not observe any further channels. In our data, the two two-body trication fragmentations are both rather rare, with $S^{2+} + CS^+$ (1.8%) being favored over $S^+ + CS^{2+}$ (1.2%). The $S^{2+} + C^+ + S$ channel (14%) is less common than the $S^{2+} + C + S^+$ channel, but still fairly prominent. Compared to the results of Eland *et al.*[64], our relative ordering of the channels is quite consistent, with the exception that in our measurements the $S^+ + C^+ + S^+$ channel is far more common. Our results also imply that the two-body channels, as well as the $S^{2+} + C^+ + S$ channel, are significantly less common than previously reported.

## IV. CONCLUSION AND OUTLOOK

We have studied the complex and multi-channel fragmentation dynamics of $CS_2$ following photoabsorption of femtosecond X-ray pulses just above the S 2p edge, produced by the FLASH FEL. Using three-dimensional velocity-map imaging and covariance analysis techniques, we extract correlated momentum distributions for a number of fragmentation channels originating from the $CS_2$ dication and trication, which are primarily populated following a single S 2p photoionization and subsequent AM decay(s). Data are collected in a regime of many detected ions per shot (∼85) and low repetition rate (10 Hz), conditions under which traditional coincidence analysis is unsuitable.

Our results provide substantial new insights into the fragmentation dynamics of $CS_2^{2+}$ and $CS_2^{3+}$. Using covariance analysis techniques, we separately interrogate 8 different fragmentation channels, extracting their KERs, ion recoil angles

and estimated branching ratios. The observed fragmentations include an intriguing dication fragmentation involving rearrangement and bond formation to yield $C^+$ and $S_2^+$, whose presence had been previously disputed[19–21]. The minor two-body fragmentation channels of the trication, producing $S^+$+ $CS^{2+}$ and $S^{2+}$+ $CS^+$ are found to exhibit very different KER distributions. The very broad distribution associated with the latter channel may indicate population of a broad range of trication electronic states that correlate to this dissociation limit.

Using recently developed native frames analysis techniques[28,30], we examine the dynamics of three-body fragmentations which yield a neutral fragment. These channels had largely evaded detailed examination in previous work[21]. Our results demonstrate the coexistence of sequential and concerted pathways for the $S^+$+ C + $S^+$ channel. For the sequential fragmentation channel, this data analysis scheme allows us to extract the KER distribution associated with both the primary and secondary dissociation. Interestingly, for this sequential channel, the KER of the primary fragmentation into $CS^+$+ $S^+$ is higher than that observed for two-body dication breakups in which the $CS^+$ does not undergo secondary dissociation. Contrastingly, the $S^+$+ $C^+$+ S channel is found to occur through concerted and asynchronous pathways, with no clear signature of a sequential fragmentation. The trication fragmentations that yield a neutral atomic product ($S^{2+}$+ $C^+$+ S and $S^{2+}$+ C + $S^+$) similarly do not show signs of sequential breakup.

The dominant breakup channel for the $CS_2^{3+}$ trication is complete Coulomb explosion into $S^+$+ $C^+$+ $S^+$. The mean KER and the overall recoil angle distribution associated with this channel agree rather well with those predicted by classical point charge simulations for the equilibrium geometry, accounting for zero point motion and geometry spread. This is attributed to the ability for inner-shell ionization to rapidly populate the $CS_2^{3+}$ trication. Dynamics on intermediate charge states are minimal and field-driven dynamics are avoided, in contrast to previous studies of $CS_2$ ionized in intense NIR fields[17]. Although exhibiting some indications of asynchronicity in the breakup, this channel is dominated by swift, concerted fragmentation.

The FLASH facility where these experiments were performed is currently undergoing technical upgrades that will further expand the scope of the methodology employed in the present work for probing the structure and ultrafast dynamics of isolated molecules[70]. A new high-repetition rate pump-probe laser will allow for pump-probe experiments at average repetition rates of $\sim$1 kHz. The greater volume of data recorded in a given experiment will enable the extension of advanced covariance (and cumulant[49,50,71]) mapping techniques to study fragmentations of more complex molecules undergoing a range of photoinduced dynamics, particularly in time-resolved Coulomb explosion imaging experiments[11,72]. Experiments performed at higher repetition-rates will also allow for the correlation of fragment ions with simultaneously detected AM electrons[21,73,74], offering rich new information by allowing the exploration of the relationship between photofragmentation mechanism and the electronic state and internal excitation of the molecular polycation. In parallel, the improved spectral purity that will be brought about through seeding the FEL will allow for more-precise resonant X-ray excitations and/or high-resolution photoelectron spectroscopy. Correlating the recorded photoelectron spectra with ion imaging data recorded simultaneously can enable the determination of channel-resolved photoelectron spectra[75], potentially in the recoil- or molecular-frame[76], sensitive probes of molecular structure and dynamics[77].

## SUPPLEMENTARY MATERIAL

The Supplementary Materials provide raw ion imaging data, details of Wigner sampling and native frame analysis, demonstrate the negligible influence of 200 nm UV pulses on the experimental results, present covariance and Dalitz plots for key channels, and list mean kinetic energy releases for all pathways.

## ACKNOWLEDGMENTS

We acknowledge DESY (Hamburg, Germany), a member of the Helmholtz Association HGF, for the provision of experimental facilities. Parts of this research were carried out at FLASH beamline BL1. Beamtime was allocated for proposal F-20200773. The research leading to this result has been supported by the project CALIPSOplus under the Grant Agreement 730872 from the EU Framework Programme for Research and Innovation HORIZON 2020. The authors gratefully acknowledge the work of the scientific and technical teams at FLASH. We acknowledge the Max Planck Society for funding the development and the initial operation of the CAMP end-station within the Max Planck Advanced Study Group at CFEL and for providing this equipment for CAMP@FLASH. The installation of CAMP@FLASH was partially funded by the BMBF Grants 05K10KT2, 05K13KT2, 05K16KT3 and 05K10KTB from FSP-302. R.F., F.A. and M.Bri gratefully acknowledge support from the Linac Coherent Light Source, SLAC National Accelerator Laboratory, which is supported by the US Department of Energy, Office of Science, Office of Basic Energy Sciences, under contract no. DE-AC02-76SF00515. F.A. is also grateful to the Alexander von Humboldt Foundation for support. P.B. was supported by the U.S. Department of Energy, Office of Science, Basic Energy Sciences (BES), Chemical Sciences, Geosciences, and Biosciences Division, AMOS Program. D.R was supported by contract no. DE-FG02-86ER13491 from the same funding agency. J.U., T.W., and M.Bu. are grateful for support from the UK EPSRC (EP/S028617/1). J.U. is also grateful to the States of Jersey for studentship funding. T.W. thanks Jesus College, Oxford and the EPSRC, for studentship funding. J.W.L.L. acknowledges financial support from the Helmholtz-ERC Recognition Award (ERC-RA-0043) of the Helmholtz Association (HGF). W.O.R. thanks the STFC XFEL Physical Sciences Hub and the university of Southampton for a PhD studentship. R.S.M.

gratefully acknowledges financial support from the Leverhulme Trust via grant RPG-2021-257. M.Bro. and C.V. gratefully acknowledge the support of EPSRC Programme Grant EP/V026690/1. I.G. was supported by an NDSEG Fellowship and by the National Science Foundation. D.M.P.H. is grateful to the Science and Technology Facilities Council, and to the UK FEL Hub for Physical Sciences, for financial support. J.Mik. gratefully acknowledges funding from the European Research Council (ERC) under the European Union's Horizon 2020 research and innovation programme within a Consolidator Grant (CoG agreement No. 101003142). A.S. and P.H. thank the NRC-CSTIP Quantum Sensors grant #QSP-075-1 for financial support. A.S. thanks the NRC-uOttawa Joint Centre for Extreme Photonics (JCEP) and the NSERC (Canada) Discovery Grant Program for financial support. H.B. acknowledges the DataX project of the Innovation Pool in the Research Field 'Matter' of the German Helmholtz Association. 

## DATA AVAILABILITY STATEMENT

The data that support the findings of this study are available from the corresponding author upon reasonable request.

[1] J. A. Reisz, N. Bansal, J. Qian, W. Zhao, and C. M. Furdui, "Effects of ionizing radiation on biological molecules—mechanisms of damage and emerging methods of detection," Antioxidants & redox signaling **21**, 260–292 (2014).

[2] C. Walsh, H. Nomura, T. Millar, and Y. Aikawa, "Chemical processes in protoplanetary disks. II. On the importance of photochemistry and X-ray ionization," The Astrophysical Journal **747**, 114 (2012).

[3] K. Siegbahn, "Electron spectroscopy for atoms, molecules, and condensed matter," Reviews of Modern Physics **54**, 709 (1982).

[4] B. E. Warren, *X-ray Diffraction* (Courier Corporation, 1990).

[5] W. a. Ackermann, G. Asova, V. Ayvazyan, A. Azima, N. Baboi, J. Bähr, V. Balandin, B. Beutner, A. Brandt, A. Bolzmann, *et al.*, "Operation of a free-electron laser from the extreme ultraviolet to the water window," Nat. Photon. **1**, 336–342 (2007).

[6] T. Wolf, R. H. Myhre, J. Cryan, S. Coriani, R. Squibb, A. Battistoni, N. Berrah, C. Bostedt, P. Bucksbaum, G. Coslovich, *et al.*, "Probing ultrafast $\pi\pi^*/n\pi^*$ internal conversion in organic chromophores via K-edge resonant absorption," Nature Communications **8**, 29 (2017).

[7] D. Mayer, F. Lever, D. Picconi, J. Metje, S. Alisauskas, F. Calegari, S. Düsterer, C. Ehlert, R. Feifel, M. Niebuhr, *et al.*, "Following excited-state chemical shifts in molecular ultrafast x-ray photoelectron spectroscopy," Nature Communications **13**, 198 (2022).

[8] Thompson *et al.*, "Shake-down spectroscopy as state- and site-specific probe of ultrafast chemical dynamics," Journal of the American Chemical Society **Accepted** (2025).

[9] R. Boll, J. M. Schäfer, B. Richard, K. Fehre, G. Kastirke, Z. Jurek, M. S. Schöffler, M. M. Abdullah, N. Anders, T. M. Baumann, S. Eckart, B. Erk, A. De Fanis, R. Dörner, S. Grundmann, P. Grychtol, A. Hartung, M. Hofmann, M. Ilchen, L. Inhester, C. Janke, R. Jin, M. Kircher, K. Kubicek, M. Kunitski, X. Li, T. Mazza, S. Meister, N. Melzer, J. Montano, V. Music, G. Nalin, Y. Ovcharenko, C. Passow, A. Pier, N. Rennhack, J. Rist, D. E. Rivas, D. Rolles, I. Schlichting, L. P. H. Schmidt, P. Schmidt, J. Siebert, N. Strenger, D. Trabert, F. Trinter, I. Vela-Perez, R. Wagner, P. Walter, M. Weller, P. Ziolkowski, S.-K. Son, A. Rudenko, M. Meyer, R. Santra, and T. Jahnke, "X-ray multiphoton-induced Coulomb explosion images complex single molecules," Nature Physics **18**, 423–428 (2022).

[10] J. Unwin, F. Allum, M. Britton, I. Gabalski, H. Bromberger, M. Brouard, P. H. Bucksbaum, T. Driver, N. Ekanayake, D. Garg, *et al.*, "X-ray induced Coulomb explosion imaging of transient excited-state structural rearrangements in $CS_2$," Communications Physics **6**, 309 (2023).

[11] T. Jahnke, S. Mai, S. Bhattacharyya, K. Chen, R. Boll, M. E. Castellani, S. Dold, U. Frühling, A. E. Green, M. Ilchen, *et al.*, "Direct observation of ultrafast symmetry reduction during internal conversion of 2-thiouracil using Coulomb explosion imaging," Nature Communications **16**, 2074 (2025).

[12] F. Légaré, K. F. Lee, I. Litvinyuk, P. Dooley, S. Wesolowski, P. Bunker, P. Dombi, F. Krausz, A. Bandrauk, D. Villeneuve, *et al.*, "Laser Coulomb-explosion imaging of small molecules," Physical Review A **71**, 013415 (2005).

[13] E. Wang, M. Gong, Z. Shen, X. Shan, X. Ren, A. Dorn, and X. Chen, "Fragmentation dynamics of $CS_2$ in collisions with 1.0 keV electrons," The Journal of Chemical Physics **149** (2018).

[14] F. Rajgara, M. Krishnamurthy, D. Mathur, T. Nishide, T. Kitamura, H. Shiromaru, Y. Achiba, and N. Kobayashi, "Fragmentation dynamics of $CS_2^{q+}$ (q= 3-10) molecular ions," Physical Review A **64**, 032712 (2001).

[15] H. Hasegawa, A. Hishikawa, and K. Yamanouchi, "Coincidence imaging of Coulomb explosion of $CS_2$ in intense laser fields," Chemical Physics Letters **349**, 57–63 (2001).

[16] A. Hishikawa, H. Hasegawa, and K. Yamanouchi, "Sequential three-body Coulomb explosion of $CS_2$ in intense laser fields appearing in momentum correlation map," Chemical physics letters **361**, 245–250 (2002).

[17] A. Hishikawa, H. Hasegawa, and K. Yamanouchi, "Nuclear dynamics on the light-dressed potential energy surface of $CS_2$ by coincidence momentum imaging," Chemical physics letters **388**, 1–6 (2004).

[18] A. Matsuda, E. J. Takahashi, and A. Hishikawa, "Time-resolved laser Coulomb explosion imaging using few-cycle intense laser pulses: Application to exploding $CS_2$ in highly charged states," Journal of Electron Spectroscopy and Related Phenomena **195**, 327–331 (2014).

[19] U. Ankerhold, B. Esser, and F. Von Busch, "Ionization and fragmentation of OCS and $CS_2$ after photoexcitation around the sulfur 2p edge," Chemical physics **220**, 393–407 (1997).

[20] M. Lavollée, "A new detector for measuring three-dimensional momenta of charged particles in coincidence," Review of scientific instruments **70**, 2968–2974 (1999).

[21] K. Saha, S. Banerjee, and B. Bapat, "Three body dissociation of $CS_2^{2+}$ subsequent to various S (2p) Auger transitions," The Journal of Chemical Physics **139** (2013).

[22] R. Guillemin, P. Decleva, M. Stener, C. Bomme, T. Marin, L. Journel, T. Marchenko, R. Kushawaha, K. Jänkälä, N. Trcera, *et al.*, "Selecting core-hole localization or delocalization in $CS_2$ by photofragmentation dynamics," Nature Communications **6**, 6166 (2015).

[23] R. Guillemin, T. Marin, M. Zmerli, C. Bomme, I. Ismail, L. Journel, T. Marchenko, O. Travnikova, M. N. Piancastelli, and M. Simon, "Concerted and sequential three-body fragmentation of deep-core-ionized carbon disulfide," Physical Chemistry Chemical Physics **25**, 183–191 (2023).

[24] N. Neumann, D. Hant, L. P. H. Schmidt, J. Titze, T. Jahnke, A. Czasch, M. Schöffler, K. Kreidi, O. Jagutzki, H. Schmidt-Böcking, *et al.*, "Fragmentation Dynamics of $CO_2^{3+}$ Investigated by Multiple Electron Capture in Collisions with Slow Highly Charged Ions," Physical review letters **104**, 103201 (2010).

[25] P. Lablanquie, I. Nenner, P. Millie, P. Morin, J. Eland, M. Hubin-Franskin, and J. Delwiche, "Single photon double ionization studies of $CS_2$ with synchrotron radiation," The Journal of Chemical Physics **82**, 2951–2960 (1985).

[26] F. Allum, C. Cheng, A. J. Howard, P. H. Bucksbaum, M. Brouard, T. Weinacht, and R. Forbes, "Multi-Particle Three-Dimensional Covariance Imaging: "Coincidence" Insights into the Many-Body Fragmentation of Strong-Field Ionized $D_2O$," Journal of Physical Chemistry Letters **12**, 8302–8308 (2021).

[27] Lam *et al.*, In Preparation (2025).

[28] J. Rajput, T. Severt, B. Berry, B. Jochim, P. Feizollah, B. Kaderiya, M. Zohrabi, U. Ablikim, F. Ziaee, K. Raju P, *et al.*, "Native frames: Disentangling sequential from concerted three-body fragmentation," Physical Review Letters **120**, 103001 (2018).

[29] J. W. McManus, T. Walmsley, K. Nagaya, J. R. Harries, Y. Kumagai, H. Iwayama, M. N. Ashfold, M. Britton, P. H. Bucksbaum, B. Downes-Ward, *et al.*, "Disentangling sequential and concerted fragmentations of molecular polycations with covariant native frame analysis," Physical

Chemistry Chemical Physics **24**, 22699–22709 (2022).

[30]T. Severt, J. Rajput, B. Berry, B. Jochim, P. Feizollah, B. Kaderiya, M. Zohrabi, F. Ziaee, K. R. P, D. Rolles, *et al.*, "Native frames: An approach for separating sequential and concerted three-body fragmentation," Physical Review A **110**, 053104 (2024).

[31]B. Erk, J. P. Müller, C. Bomme, R. Boll, G. Brenner, H. N. Chapman, J. Correa, S. Düsterer, S. Dziarzhytski, S. Eisebitt, *et al.*, "CAMP@FLASH: an end-station for imaging, electron-and ion-spectroscopy, and pump-probe experiments at the FLASH free-electron laser," J. Synchrotron Radiat. **25**, 1529–1540 (2018).

[32]I. Gabalski, F. Allum, I. Seidu, M. Britton, G. Brenner, H. Bromberger, M. Brouard, P. H. Bucksbaum, M. Burt, J. P. Cryan, *et al.*, "Time-resolved X-ray photoelectron spectroscopy: Ultrafast dynamics in $CS_2$ probed at the S 2p edge," The Journal of Physical Chemistry Letters **14**, 7126–7133 (2023).

[33]T. Poikela, J. Plosila, T. Westerlund, M. Campbell, M. De Gaspari, X. Llopart, V. Gromov, R. Kluit, M. Van Beuzekom, F. Zappon, *et al.*, "Timepix3: a 65K channel hybrid pixel readout chip with simultaneous ToA/ToT and sparse readout," Journal of Instrumentation **9**, C05013 (2014).

[34]H. Bromberger, C. Passow, D. Pennicard, R. Boll, J. Correa, L. He, M. Johny, C. C. Papadopoulou, A. Tul-Noor, J. Wiese, *et al.*, "Shot-by-shot 250 kHz 3D ion and MHz photoelectron imaging using Timepix3," Journal of Physics B: Atomic, Molecular and Optical Physics **55**, 144001 (2022).

[35]A. Zhao, M. van Beuzekom, B. Bouwens, D. Byelov, I. Chakaberia, C. Cheng, E. Maddox, A. Nomerotski, P. Svihra, J. Visser, *et al.*, "Coincidence velocity map imaging using Tpx3Cam, a time stamping optical camera with 1.5 ns timing resolution," Review of Scientific Instruments **88** (2017).

[36]D. A. Dahl, *SIMION 8.1 User Manual*, Idaho National Laboratory (2000).

[37]M. R. F. Siggel, C. Field, L. J. Sæthre, K. J. Bøorve, and T. D. Thomas, "High resolution photoelectron spectroscopy of sulfur 2p electrons in $H_2S$, $SO_2$, $CS_2$, and OCS," The Journal of Chemical Physics **105**, 9035–9039 (1996).

[38]K. Tiedtke, J. Feldhaus, U. Hahn, U. Jastrow, T. Nunez, T. Tschentscher, S. V. Bobashev, A. A. Sorokin, J. B. Hastings, S. Möller, L. Cibik, A. Gottwald, A. Hoehl, U. Kroth, M. Krumrey, H. Schöppe, G. Ulm, and M. Richter, "Gas detectors for X-ray lasers," J. Appl. Phys. **103**, 094511 (2008).

[39]C. Behrens, N. Gerasimova, C. Gerth, B. Schmidt, E. Schneidmiller, S. Serkez, S. Wesch, and M. Yurkov, "Constraints on photon pulse duration from longitudinal electron beam diagnostics at a soft x-ray free-electron laser," Physical Review Accel. Beams. **15**, 030707 (2012).

[40]J. Mikosch and S. Patchkovskii, "Coincidence and covariance data acquisition in photoelectron and-ion spectroscopy. I. Formal theory," J. Mod. Opt. **60**, 1426–1438 (2013).

[41]J. Mikosch and S. Patchkovskii, "Coincidence and covariance data acquisition in photoelectron and-ion spectroscopy. II. Analysis and applications," J. Mod. Opt. **60**, 1439–1451 (2013).

[42]C. Cheng, L. J. Frasinski, G. Moǧol, F. Allum, A. J. Howard, D. Rolles, P. H. Bucksbaum, M. Brouard, R. Forbes, and T. Weinacht, "Multiparticle Cumulant Mapping for Coulomb Explosion Imaging," Physical Review Letters **130**, 093001 (2023).

[43]T. Walmsley, J. W. McManus, Y. Kumagai, K. Nagaya, J. Harries, H. Iwayama, M. N. Ashfold, M. Britton, P. H. Bucksbaum, B. Downes-Ward, *et al.*, "The role of momentum partitioning in covariance ion imaging analysis," The Journal of Physical Chemistry A **128**, 4548–4560 (2024).

[44]T. Walmsley, F. Allum, J. R. Harries, Y. Kumagai, S. Lim, J. McManus, K. Nagaya, M. Britton, M. Brouard, P. Bucksbaum, *et al.*, "Distinguishing the XUV-induced Coulomb explosion dynamics of iodobenzene using covariance analysis," Journal of Physics B: Atomic, Molecular and Optical Physics **57**, 235101 (2024).

[45]L. Frasinski, K. Codling, and P. Hatherly, "Covariance mapping: A correlation method applied to multiphoton multiple ionization," Science **246**, 1029–1031 (1989).

[46]C. S. Slater, S. Blake, M. Brouard, A. Lauer, C. Vallance, J. J. John, R. Turchetta, A. Nomerotski, L. Christensen, J. H. Nielsen, *et al.*, "Covariance imaging experiments using a pixel-imaging mass-spectrometry camera," Physical Review A **89**, 011401 (2014).

[47]J. D. Pickering, K. Amini, M. Brouard, M. Burt, I. J. Bush, L. Christensen, A. Lauer, J. H. Nielsen, C. S. Slater, and H. Stapelfeldt, "Communication: Three-fold covariance imaging of laser-induced Coulomb explosions," The Journal of Chemical Physics **144**, 161105 (2016).

[48]F. Allum, "PyCorrCPI - corelation analysis for charged-particle imaging experiments," `https://github.com/f-allum/PyCorrCPI` (2024).

[49]C. Cheng, L. J. Frasinski, G. Moǧol, F. Allum, A. J. Howard, P. H. Bucksbaum, R. Forbes, and T. Weinacht, "Multiparticle cumulant mapping for Coulomb explosion imaging: Calculations and algorithm," Physical Review A **109**, 042802 (2024).

[50]S. Patchkovskii and J. Mikosch, "Statistical theory of cumulant mapping in an imperfect apparatus," Physical Review A **111**, 043108 (2025).

[51]L. Frasinski, V. Zhaunerchyk, M. Mucke, R. J. Squibb, M. Siano, J. H. Eland, P. Linusson, P. Vd Meulen, P. Salén, R. Thomas, *et al.*, "Dynamics of Hollow Atom Formation in Intense X-Ray Pulses Probed by Partial Covariance Mapping," Physical Review Letters **111**, 073002 (2013).

[52]V. Zhaunerchyk, M. Mucke, P. Salén, P. Vd Meulen, M. Kaminska, R. Squibb, L. Frasinski, M. Siano, J. Eland, P. Linusson, *et al.*, "Using covariance mapping to investigate the dynamics of multi-photon ionization processes of Ne atoms exposed to X-FEL pulses," Journal of Physics B: Atomic, Molecular and Optical Physics **46**, 164034 (2013).

[53]V. Zhaunerchyk, L. J. Frasinski, J. H. D. Eland, and R. Feifel, "Theory and simulations of covariance mapping in multiple dimensions for data analysis in high-event-rate experiments," Physical Review A **89**, 053418 (2014).

[54]L. J. Frasinski, "Covariance mapping techniques," Journal of Physics B: Atomic, Molecular and Optical Physics **49**, 152004 (2016).

[55]F. Allum, "PyCESIM - Python package for the classical simulation of Coulomb explosion," `https://github.com/f-allum/PyCESim` (2024).

[56]J. P. Dahl and M. Springborg, "The Morse oscillator in position space, momentum space, and phase space," The Journal of Chemical Physics **88**, 4535–4547 (1988).

[57]L. Sun and W. L. Hase, "Comparisons of classical and Wigner sampling of transition state energy levels for quasiclassical trajectory chemical dynamics simulations," The Journal of Chemical Physics **133** (2010).

[58]S. Mai, P. Marquetand, and L. González, "Nonadiabatic dynamics: The SHARC approach," Wiley Interdisciplinary Reviews: Computational Molecular Science **8**, e1370 (2018).

[59]P. Wang and C. Vidal, "Dissociation of multiply ionized carbonyl sulfide due to electron impact," The Journal of Chemical Physics **118**, 5383–5389 (2003).

[60]S. Zhao, B. Jochim, P. Feizollah, J. Rajput, F. Ziaee, K. R. P, B. Kaderiya, K. Borne, Y. Malakar, B. Berry, *et al.*, "Strong-field-induced bond rearrangement in triatomic molecules," Physical Review A **99**, 053412 (2019).

[61]M. Jarraya, M. Wallner, S. B. Yaghlane, E. Olsson, V. Ideböhn, R. J. Squibb, J. Palaudoux, G. Nyman, M. M. Al-Mogren, J. H. Eland, *et al.*, "Doubly ionized OCS bond rearrangement upon fragmentation–experiment and theory," Physical Chemistry Chemical Physics **25**, 19435–19445 (2023).

[62]S. Taylor, J. Eland, and M. Hochlaf, "Fluorescence from the cs22+ dication: Theory and experiment," Chemical physics **330**, 16–25 (2006).

[63]M. Kato, Y. Morishita, M. Oura, H. Yamaoka, Y. Tamenori, K. Okada, T. Matsudo, T. Gejo, I. Suzuki, and N. Saito, "Absolute photoionization cross sections with ultra-high energy resolution for Ar, Kr, Xe and $N_2$ in inner-shell ionization regions," Journal of Electron Spectroscopy and Related Phenomena **160**, 39–48 (2007).

[64]J. Eland, C. Rigby, E. Andersson, J. Palaudoux, L. Andric, F. Penent, P. Linusson, L. Hedin, L. Karlsson, J.-E. Rubensson, *et al.*, "Spectra of the triply charged ion $CS_2^{3+}$ and selectivity in molecular Auger effects," The Journal of Chemical Physics **132**, 104311 (2010).

[65]M. Hochlaf, G. Chambaud, and P. Rosmus, "Theoretical study of the electronic states of $CS_2^{++}$," The Journal of Chemical Physics **108**, 4047–4053 (1998).

[66]J. Eland, "The dynamics of three-body dissociations of dications studied by the triple coincidence technique pepipico," Molecular Physics **61**, 725–745 (1987).

[67]T. Severt, Z. L. Streeter, W. Iskandar, K. A. Larsen, A. Gatton, D. Trabert, B. Jochim, B. Griffin, E. G. Champenois, M. M. Brister, *et al.*, "Step-by-step state-selective tracking of fragmentation dynamics of water dications by momentum imaging," Nature Communications **13**, 5146 (2022).

[68]J. W. McManus, F. Allum, J. Featherstone, C.-S. Lam, and M. Brouard, "Two-dimensional projected-momentum covariance mapping for coulomb explosion imaging," The Journal of Physical Chemistry A **128**, 3220–3229 (2024).

[69]P. Franceschi, D. Ascenzi, P. Tosi, R. Thissen, J. Žabka, J. Roithova, C. L. Ricketts, M. De Simone, and M. Coreno, "Dissociative double photoionization of $N_2$ using synchrotron radiation: appearance energy of the $N_2^+$ dication," The Journal of chemical physics **126** (2007).

[70]M. Beye, M. Gühr, I. Hartl, E. Plönjes, L. Schaper, S. Schreiber, K. Tiedtke, and R. Treusch, "FLASH and the FLASH2020+ project—current status and upgrades for the free-electron laser in Hamburg at DESY," The European Physical Journal Plus **138**, 193 (2023).

[71]L. J. Frasinski, "Cumulant mapping as the basis of multi-dimensional spectrometry," Phys. Chem. Chem. Phys. **24**, 20776–20787 (2022).

[72]F. Allum, M. Burt, K. Amini, R. Boll, H. Köckert, P. K. Olshin, S. Bari, C. Bomme, F. Brauße, B. Cunha de Miranda, S. Düsterer, B. Erk, M. Géléoc, R. Geneaux, A. S. Gentleman, G. Goldsztejn, R. Guillemin, D. M. P. Holland, I. Ismail, P. Johnsson, L. Journel, J. Küpper, J. Lahl, J. W. L. Lee, S. Maclot, S. R. Mackenzie, B. Manschwetus, A. S. Mereshchenko, R. Mason, J. Palaudoux, M. N. Piancastelli, F. Penent, D. Rompotis, A. Rouzée, T. Ruchon, A. Rudenko, E. Savelyev, M. Simon, N. Schirmel, H. Stapelfeldt, S. Techert, O. Travnikova, S. Trippel, J. G. Underwood, C. Vallance, J. Wiese, F. Ziaee, M. Brouard, T. Marchenko, and D. Rolles, "Coulomb explosion imaging of $CH_3I$ and $CH_2ClI$ photodissociation dynamics," The Journal of Chemical Physics **149**, 204313 (2018).

[73]U. Alkemper and F. Von Busch, "Auger and electron/double-ion coincidence spectroscopy of sulfur (2p)-ionized cs2 molecules," Journal of electron spectroscopy and related phenomena **93**, 115–125 (1998).

[74]T. A. Field and J. H. Eland, "The fragmentation dynamics of cs22+," Chemical physics letters **303**, 144–150 (1999).

[75]F. Allum, V. Music, L. Inhester, R. Boll, B. Erk, P. Schmidt, T. M. Baumann, G. Brenner, M. Burt, P. V. Demekhin, *et al.*, "A localized view on molecular dissociation via electron-ion partial covariance," Communications chemistry **5**, 42 (2022).

[76]G. Kastirke, M. S. Schöffler, M. Weller, J. Rist, R. Boll, N. Anders, T. M. Baumann, S. Eckart, B. Erk, A. De Fanis, *et al.*, "Photoelectron diffraction imaging of a molecular breakup using an x-ray free-electron laser," Physical Review X **10**, 021052 (2020).

[77]K. Yoshikawa, M. Kanno, H. Xue, N. Kishimoto, S. Goto, F. Ota, Y. Tamura, F. Trinter, K. Fehre, L. Kaiser, *et al.*, "Time-resolved photoelectron diffraction imaging of methanol photodissociation involving molecular hydrogen ejection," Physical Chemistry Chemical Physics **26**, 25118–25130 (2024).